THE JOURNAL OF PHYSICAL CHEMISTRY C

Article

pubs.acs.org/JPCC

Crystalline Silicon under Acoustic Cavitation: From Mechanoluminescence to Amorphization

Matthieu Virot,*[†,‡] Rachel Pflieger,[†] Ekaterina V. Skorb,[‡] Johann Ravaux,[†] Thomas Zemb,[†] and Helmuth Möhwald[‡]

[†]Institut de Chimie Séparative de Marcoule (ICSM), UMR 5257 CEA/CNRS/UM2/ENCSM, ICSM Site de Marcoule, BP 17171, 30207 Bagnols-sur-Cèze, France

[‡]Max Planck Institute of Colloids and Interfaces (MPIKGF), Wissenschaftspark Potsdam-Golm, Am Mühlenberg 1 OT Golm, 14476 Potsdam, Germany

Supporting Information

ABSTRACT: The physicochemical behavior of crystalline silicon under acoustic cavitation is investigated in water sparged with argon at low temperature (10 and 20 °C). Surprisingly, spectroscopic investigations reveal that argon (bubbling continuously through the liquid phase during experiments) can be ultrasonically excited via mechanoluminescence, i.e., emission of light caused by mechanical action on a solid. This phenomenon is highlighted for the first time on an extended solid surface using these conditions and results from an interaction between the acoustically generated bubbles and the Si surface. The concomitant physical and chemical transformations induced at the solid−liquid interface are investigated (SEM, AFM) to characterize the generated stress and defects in combination with the roughness and wettability increases (evolving from ∼46° to ∼4°). Phase transformations of the Si lattice are observed (Raman spectroscopy, TEM) evidencing the complex stress state induced by acoustic cavitation in the Si crystal structure. The mechanisms involved during Si sonication are discussed.

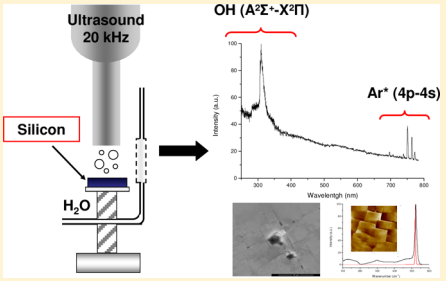

1. INTRODUCTION

With the current prospects toward development of specific materials and methodologies offering a wide control over their physical and chemical properties, ultrasound appears to be a promising tool allowing several possibilities for manipulation of surfaces at the atomic level and synthesis of new nanostructures.[1−4] Ultrasound benefits are generally attributed to the acoustic cavitation phenomenon, i.e., nucleation, growth, and rapid implosive collapse of acoustically generated microbubbles in liquids. Acoustic cavitation is able to locally generate extreme transient conditions of ∼5000 K and ∼1000 bar ("hot spots"), going along with formation of excited species and free radicals (e.g., via homolytic dissociation of water) and a possible light emission propagating from the UV to the near-IR, referred to as sonoluminescence.[1,2,5−7] In heterogeneous systems, acoustic cavitation goes with generation of shock waves and microjets that can affect a solid surface in view of specific applications such as cleaning, extracting, soldering, etc.[5−8] Over the past decade, scientific interest in sonication of heterogeneous systems has considerably increased and focused on various topics such as, for instance, preparation of nanoparticles,[1,2,4] catalysis,[9] preparation of porous and nanostructured materials,[2,10] nucleation processes,[11,12] sonophotoluminescence,[13] etc. In 2006, Eddingsaas and Suslick evidenced the possible triggering of mechanoluminescence (i.e., light emission caused by application of mechanical energy on a solid) during sonication of organic crystal slurries.[14−16] The high-velocity interparticle collisions created during sonication (20 kHz) of suspensions of sucrose and resorcinol crystals in organic solvents allowed spectroscopic observation of gas discharges and crystal luminescence usually observed for triboluminescence.[14−16] This emission of light was attributed to a piezoelectrification of the newly created surfaces during fracture and was later investigated by other authors on lanthanide crystals sonicated in perfluorodecalin and undecane.[17,18]

Cavitation effects at the solid−liquid interface have not been totally deciphered yet, and an understanding of the mechanisms generated at the interface is still an important challenge. Despite the numerous investigations dealing with ultrasonic treatment of materials, the behavior of silicon under acoustic cavitation remains a topic scarcely reported in the literature. However, Si is an industrial key material that has been widely considered in microelectronic technology, integrated circuits, and optoelectronic devices.[19−21] In addition, modification of crystalline Si into amorphous silicon (a-Si) and polycrystalline silicon (poly-Si) represents a challenge of paramount importance in the development of, for instance, less expensive solar cells, image sensors, or thin film transistors.[10,21−24] Several techniques have been devoted to deposition or transformation of these Si structures, such as plasma-enhanced chemical vapor deposition,[25] electron irradiation,[26] indentation,[27−29] plasma arc processing,[30] microcutting,[31] ball milling,[32,33] etc. The few studies related to sonication of Si were principally focused on

Received: June 1, 2012
Published: June 21, 2012

surface cleaning[34,35] or the luminescence behavior of poly-Si and porous Si.[36−39] However, an original and environmentally friendly way of Si modification, using ultrasonic treatment in view of development of porous luminescent structures, was recently described in the literature.[10] Sonication of Si in the presence of reducing agents was found to dramatically influence the nature of luminescent centers. As such, the nonequilibrium conditions provided by acoustic cavitation phenomena appear to represent an original alternative for surface modification of Si-based materials. It is thus interesting to evaluate the potential of high-intensity ultrasound in this area aiming at controlling at the small scale the Si physicochemical properties such as wetting, porosity, morphology, optoelectronic properties, etc.

This work comes within the scope of a currently evolving domain dealing with engineered interfaces of acoustically generated cavitation bubbles for manipulation of surfaces at the small scale. This paper contributes to the understanding of the mechanisms involved at the surface of crystalline Si during acoustic cavitation (20 kHz) in aqueous solution under argon bubbling. Spectroscopic effects developed near the surface of the Si wafer during sonication are investigated. The concomitant physicochemical transformations occurring at the Si surface and within its structure are described and studied during the early stage of the erosion process. The mechanisms involved in the various highlighted phenomena are discussed.

2. EXPERIMENTAL SECTION

Materials. Crystalline silicon wafers (Prime CZ, N−As, one side polished, thickness 850 μm), with a (100) surface crystallographic orientation, were purchased from Siltronix (Archamps, France). They were cut into the appropriate diameter to fit the Teflon sample holder used for sonication experiments. Special care was taken to use smooth samples, devoid of apparent defects that could play a role during sonication. The various experiments were performed in deionized Milli-Q water (resistivity higher than 18.2 MΩ·cm at 25 °C).

Sonication and Sonoluminescence. In typical experiments, the Si samples were loaded on a homemade sample holder, allowing maintaining a controlled and reproducible distance from the ultrasonic probe.[13] This sample holder is manufactured from Teflon and allows a flat angle treatment of the Si surface. The sample is sonicated at 20 kHz using a 1 cm^2 titanium horn (Vibra-cell, Sonics & Materials, 750 W) mounted on top of a cylindrical reactor and fixed with a watertight Teflon ring, allowing its reproducible immersion into deionized water (250 mL). Experiments were performed at constant temperature (10 or 20 °C) using a Lauda RE 210 cryostat and measured with a thermocouple inserted into the reactor. Sonication was performed under argon bubbling (100 mL min^{-1}) through the solution 20 min before sonication and during the whole experiments. In order to ensure a maximal effect of cavitation, the tip of the probe is regularly changed.

For sonoluminescence investigations, experiments were performed using the devices described elsewhere.[13,40] Briefly, the light emitted within the reactor is collected through a quartz window and imaged onto the slit (0.1 mm) of a spectrometer (SP 2356i, Roper Scientific; gratings 300 gr/mm blz. 300 and 150 gr/mm blz. 500) coupled to a CCD camera (Spec10-100BR with UV coating, Roper Scientific) cooled with liquid nitrogen. Spectra are recorded with appropriate filters from 250 to 800 nm acquired during 300 s and corrected for background noise and quantum efficiencies of gratings and CCD.[40] The acoustic power P_{ac} (W mL^{-1}) or ultrasonic intensity I_{ac} (W cm^{-2}) delivered to the solution was measured using the conventional thermal probe method. Sonochemical production of H_2O_2 was measured spectrophotometrically as a chemical way of cavitation control using Ti(IV) in ∼2 M HNO_3−0.01 M $[N_2H_5][NO_3]$ at λ_{max} (ε) = 410 nm (780 cm^{-1} M^{-1}).[41] Under these conditions, with an applied acoustic intensity of I_{ac} = 32 W cm^{-2}, the formation rate of H_2O_2 was measured to be ∼4.2 × 10^{-1} μM min^{-1}, which is in agreement with the literature.[8]

Characterization. Different samples were studied using a scanning electron microscope (SEM, FEI QUANTA 200 ESEM FEG) coupled with energy-dispersive X-ray spectroscopy (EDX, Bruker SDD 5010). To characterize the topography of the various samples, atomic force microscopy (AFM) was applied to obtain quantitative data about the roughness, height profile, and created hole depths of the sonicated surfaces. Measurements were carried out in air at room temperature using a D3100 Nanoscope IIIa MultiMode microscope (Digital instruments/Veeco, Inc., Santa Barbara, CA) in tapping mode with silicon cantilevers (Nanoworld, Neuchâtel, Switzerland). The typical resonance frequency of the cantilevers was 285 kHz, and the spring constant was 42 N m^{-1}. In this study, recorded images possess a scan area of 40 × 40 μm^2. Analyses and treatments of the various images were carried out with the software provided by the manufacturer.

The surface of the different Si wafers was studied using a Raman microspectrometer (μ-Raman). The apparatus (Horiba-Jobin Yvon Aramis) is equipped with an edge filter and a He−Ne laser (λ = 633 nm). The laser beam is focused on the Si samples using a microscope (Olympus BX 41) with a ×100 magnification, resulting in a spot of about 1 μm^2. Spectra were collected between 100 and 1100 cm^{-1} with usual averaged measurements of 4 scans of 8 s each. The apparent contact angle of the Si wafers was investigated with deionized Milli-Q water droplets using a contact angle meter (Software DSA 1, Krüss GmbH, Hamburg, Germany). The reported contact angles are obtained from a mean average of ∼10 measurements. Transmission electron microscopy (TEM) was used to investigate the structural modification and the local orientations of the Si structures using a Zeiss EM 912 Omega (Carl Zeiss AG, Germany) operating at 120 kV and equipped with an electron-diffraction unit. For analyses, samples were ultramicrotomed (Leica EM FC6) or gently broken before being deposited with ethanol on a carbon-coated copper grid.

3. RESULTS AND DISCUSSION

The 20 kHz sonication of the surface of a water-immersed silicon wafer in the presence of argon (bubbling continuously through the liquid phase) leads to spectroscopic observation of several emission lines (Figure 1). Spectra are constituted by a broad continuum superimposed with particular emission peaks. The continuum is typical for multibubble water sonoluminescence and found to be in agreement with previous investigations.[13,40] It is generally considered that the continuum results from a combination of bremsstrahlung, recombination of H and OH° species, deexcitation of water molecules, and/or $OH(B^2\Sigma^+-A^2\Sigma^+)$ emission.[40] The intense emission lines around 310 nm are attributed to $OH(A^2\Sigma^+-X^2\Pi)$ transitions; these excited OH° radicals result from the homolytic dissociation of water molecules inside the cavitation bubbles. The observed lines can be decomposed into several vibrational transitions, e.g., the 0−0 transition at 310 nm, the 1−0 between ∼290 and 300 nm, and the 0−1 at ∼340 nm.[13,40] The most

dx.doi.org/10.1021/jp305375r | J. Phys. Chem. C 2012, 116, 15493−15499

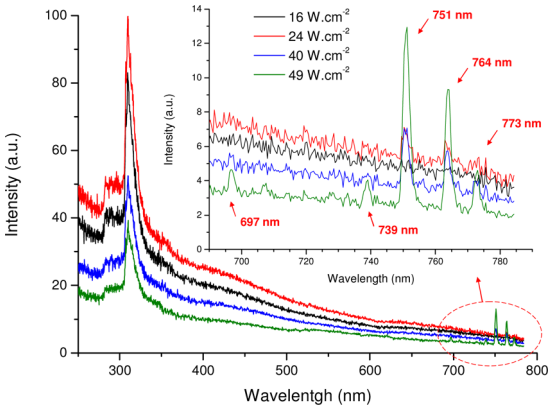

Figure 1. Normalized sonoluminescence spectra obtained during sonication of a Si wafer in H_2O using different acoustic intensities (10 ± 1 °C, Ar, ∼2 mm from the sonotrode, focusing near the surface). (Inset) Magnification of the 690−790 nm region.

interesting features extend in the near-IR range, where several emission lines are observed at 697, 739, 751, 764, and 773 nm. These lines are attributed in agreement with the literature to the 4p−4s manifold transitions of the excited argon atom (Ar*).[42,43] The relevant region can also be observed in Supporting Information Figure SI.1, where the background of the different spectra was subtracted in order to appreciate the relative intensity of the main Ar* and $OH(A^2\Sigma^+-X^2\Pi)$ transitions versus the applied acoustic intensity.

According to Figure 1 and Supporting Information Figure SI.1, observation of Ar* transitions clearly depends on the applied acoustic intensity. Application of an acoustic intensity of ∼16 W cm^{-2} does not permit observation of any significant Ar* line; however, a threshold intensity of 24 W cm^{-2} is observed. Thereafter, the intensity of the different Ar* lines increases almost linearly with the applied acoustic intensity, while the intensity of $OH(A^2\Sigma-X^2\Pi)$ transitions decreases (Figure 1 and Supporting Information Figure SI.1). The decrease of the $OH(A^2\Sigma-X^2\Pi)$ transitions can be explained by a modification of the geometry of the cavitation cloud of bubbles as a function of the applied acoustic intensity. It is important to mention that sonication of pure water with argon bubbling continuously in the liquid phase did not lead to Ar* observation; similarly, sonication of a silica surface in water did not permit the observation of excited species emission (except that of OH* from water sonoluminescence). Furthermore, spectra observed with Si result from optimization of the experimental parameters: sonication at a high distance from the sonotrode did not permit observation of any Ar* line; a ∼2 mm probe−sample distance was necessary to obtain relevant spectra. It is important to note that the physical effects (e.g., sonication erosion) of a solid surface highly depend on the distance between the surface and the sonotrode.[8,13] An increase of this distance drops dramatically the surface-induced cavitation effects. These observations permit one to evidence the link between the sonicated solid surface and Ar* observation.

The observed Ar* excitation level (>13 eV above the ground state) most probably results from a dielectric breakdown occurring during formation of cracks in Si crystals during sonication.[14−18] Ar* emission can therefore be attributed to gas discharges. Combination of the experimental settings with the observed spectroscopic variations evidence a direct relationship with the mechanical stimuli created at the Si−water interface. In consequence, the observed phenomenon is attributed to mechanoluminescence, i.e., light emission resulting from mechanical deformation of a solid.[44] It is important to emphasize that this mechanism of excitation differs from that recently discovered during sonication of suspensions of piezoelectric organic crystals (i.e., triboluminescence, see Introduction).[14−18] Indeed, the here-described emission of Ar* does not involve collisions with particles or piezoelectrification of the surface since we consider an extended solid surface and a centrosymmetric crystal.

The ultrasonically induced stress state at the surface of the sample was investigated using different techniques. The first observation (optical microscopy) revealed that deformation of the surface is very slow and presents a long incubation period of cavitation erosion. Higher magnification (SEM) shows that the Si wafer undergoes dramatic changes at the small scale under sonication (Figure 2). An increasing density of cracks and small pits is appearing with the duration and intensity of the acoustic cavitation. The size of the primary holes was measured using AFM and found to be about ∼0.5−2 μm thick and ∼30−70 nm deep. The erosion mechanism is in good agreement with previous observations on glass surfaces, although the depth of

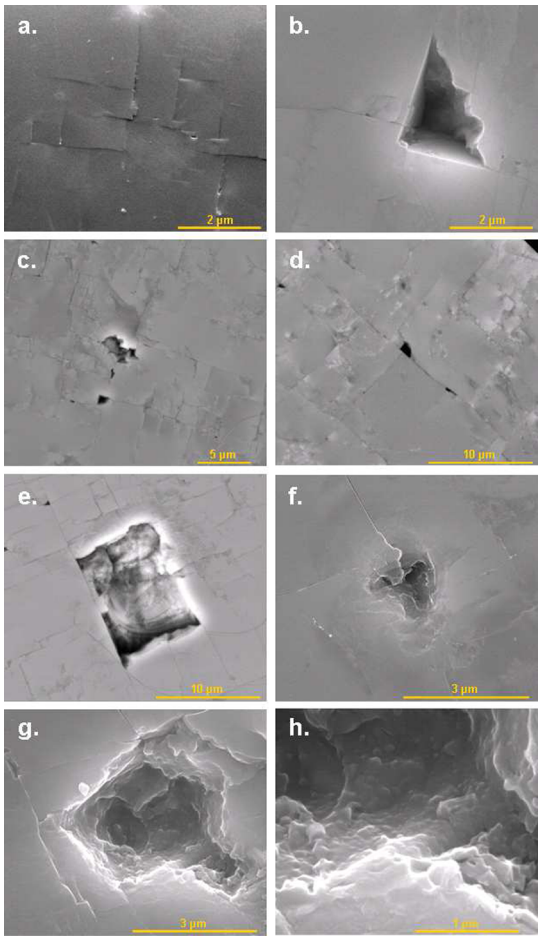

Figure 2. SEM observation of the silicon surface evidencing the crystallographic propagation of cracks and defect evolution after (a) 5 h of sonication, (b and c) 7 h of sonication, (d) 9 h of sonication, (e) 12 h of sonication, and (f−h) 15 h of sonication. Conditions: I_{ac} = 32 W cm^{-2}, Ar, 20 °C, H_2O, V = 250 mL. Note the general rectilinear geometry (a−e) and the plastic area (e−h) of some created defects suggesting a local brittle-to-ductile transition.

dx.doi.org/10.1021/jp305375r | J. Phys. Chem. C 2012, 116, 15493−15499

the holes is in comparison smaller for Si.[8] This might be the result of the hardness of the sample supposed to be stronger for Si. Prolonged sonication allows acceleration of the erosion phenomenon (an incubation period of ∼4 h appears necessary), which leads to generation of secondary effects characterized by the presence of larger eroded areas (∼5−10 μm) and the intersection of the cracks (Figure 2d).

The fissures were found to propagate straight and intersect with 90° angles, which is in agreement with the cubic crystal orientation of (100) Si wafers (Figures 2 and 3 and Supporting

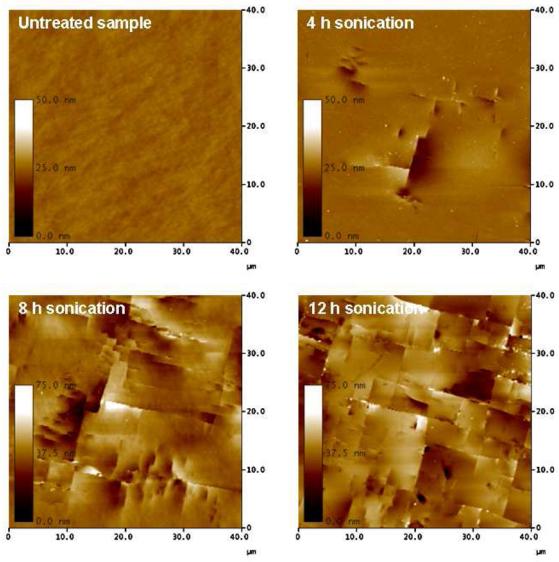

Figure 3. AFM topographic measurements of a silicon surface for different sonication times at I_{ac} = 32 W cm^{-2} (Ar, 20 °C, H_2O, V = 250 mL).

Information Figures SI.2 and SI.3). The observed perfect cleavages result from an interaction with the bulk material and therefore testify the extreme conditions generated by acoustic cavitation. SEM observations of the created defects suggest the coexistence of two modes of fracture at the surface of the sample. Indeed, some created defects exhibit an erosion in agreement with the brittle nature of crystalline Si at room temperature (linear cracks and defects as observed in Figure 2a−e), while other areas suggest the presence of plastically deformed areas (Figure 2e−h), evidencing a local disorder as observed in ref 36. Finally, note the presence of surface deformations which were revealed by SEM and AFM investigations (Figures 2 and 3, and Supporting Information Figure SI.3). These features are also increasing with the sonication time and intensity and characterized by height differences when considering the two sides of a crack (see the AFM scan line in Supporting Information Figure SI.2).

AFM topographic measurements allow one to monitor the morphological evolution of the sonicated Si wafer for long periods of treatment and demonstrate the relative increase of the roughness of the surface (Figure 3). The corresponding surface roughness was quantified (Figure 4) using R_a (arithmetic average of the absolute values of the surface height deviations measured from the mean plane) and R_q (root-mean-square average of height deviations taken from the mean image data plane) parameters.[8] The initial surface was found to be totally flat, devoid of defects, with a measured roughness lower than 1 nm. After 4 h of sonication, the surface reaches a

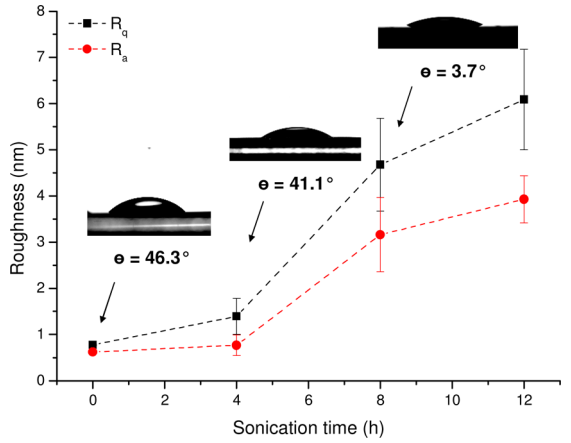

Figure 4. Measurements of the roughness and contact angle of the silicon wafer surface as a function of the sonication time (Ar, 20 °C, I_{ac} = 32 W cm^{-2}, H_2O, V = 250 mL).

roughness of 0.77 and 1.39 nm for R_a and R_q, respectively, while 12 h of sonication leads to a roughness around 3.9 and 6.1 nm for R_a and R_q, respectively. The roughness of the Si surface is therefore increasing with sonication time for both parameters, which is in agreement with SEM measurements. In comparison with the measurements performed on various glass and metallic surfaces in previous investigations, the erosion damage and roughness increases observed for Si are less pronounced and quite slow.[8,45] These observations emphasize the better cavitation erosion resistance of Si and confirm the long incubation period observed for Si with microscopy.

The corresponding water contact angle measured on the various samples shows an important increase of the hydrophilicity of the Si surface going from ∼46° to ∼4° within ∼8 h of sonication (Figure 4). The contact angle is very sensitive to local physical transformations of a surface. Therefore, the created superhydrophilicity of the surface may be the result of an increase of the density of hydroxyl groups at the newly created surfaces or to an inverse lotus effect, since AFM showed an increase of roughness. The nonlinear behavior of the contact angle and roughness versus the sonication time suggests a possible concomitant contribution of both physical (roughness) and chemical (density of OH groups) phenomena.

In addition to local chemistry, the strains ultrasonically generated at the Si surface may modify the interatomic distances and lattice vibration frequencies of the crystalline structure.[32,33] μ-Raman spectroscopy appears to be a candidate of choice to investigate the mechanical stress and local atomic arrangement at the surface of the wafer. At atmospheric pressure, the untreated Si wafer exhibits a cubic diamond structure (space group $Fd3m$) characterized by a narrow Raman peak at ∼521.5 cm^{-1} and corresponding to the transversal optical (TO) phonon of the crystalline c-Si (phase conventionally labeled Si−I).[27−30] This peak was found to be predominant in all of our Raman spectra and can be observed in Figure 5 (depicted in red for all spectra); it corresponds to the triply degenerated optical phonon in the center of the Brillouin zone.[27−30,46] After sonication, some spectra were found to present a broadened TO c-Si band with a measured full width at half-maximum (FWHM) up to Γ_c ≈7.1 cm^{-1} (against ∼3.4 cm^{-1} for the nontreated c-Si, Figure 5a). TO peak broadening can be attributed not only to an increase in the density of defects within the crystals but also to a phonon

dx.doi.org/10.1021/jp305375r | J. Phys. Chem. C 2012, 116, 15493−15499

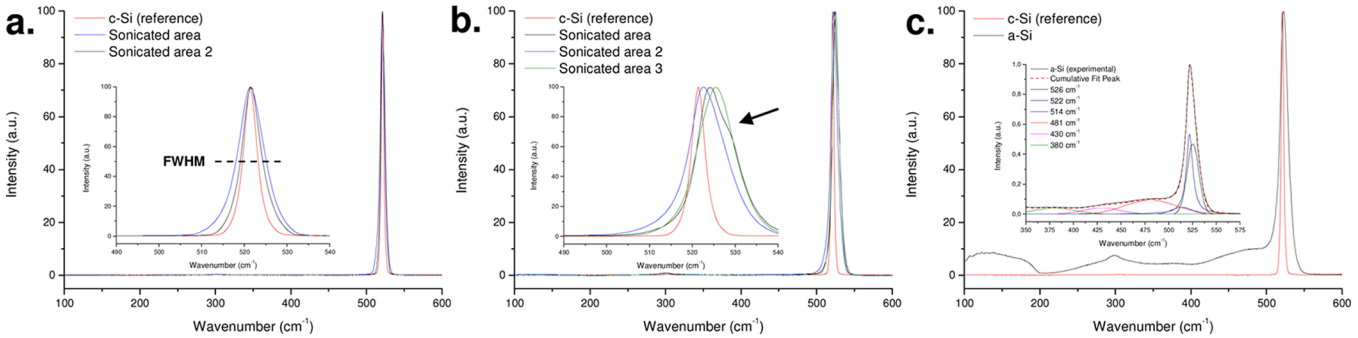

Figure 5. Raman spectra measured around localized defects after 8 h of sonication (I_{ac} = 32 W cm^{-2}, Ar, 20 °C, H_2O, V = 250 mL). For all spectra, the crystalline reference sample c-Si is depicted in red. Spectra characterize different features: (a) broadening of the TO c-Si peak, (b) broadening, frequency shift, and quasi-split of the TO peak, and (c) formation of an amorphous structure. Insets of a and b are magnification of the relevant zone; inset of c is a deconvolution of the amorphous spectrum between 350 and 575 nm.

confinement effect resulting from the presence of polycrystalline Si (poly-Si).[23,27−29,32,33,47] Other sonicated areas were found to present a high-frequency shift and showed the apparition of a shoulder on the TO c-Si peak (black arrow in Figure 5b). These features are representative for an anisotropic compressive stress going along with a lattice deformation and leading to removal of the degeneracy of the Raman modes.[47,48] The observed frequency shift is known to be influenced by the mechanical stress generated in the crystalline structure and reflects a discrepancy in the distribution of the bond length of the sonicated Si.[32,33]

It is generally admitted that a compressive stress results in a frequency increase of the Raman bands, whereas a tensile stress will downshift the Raman frequency.[30,47,48] In our case, the upward shift ($\Delta\omega$) of the Si peak, in comparison to the unstressed Si, confirms a compressive strain in the lattice. Assuming a uniaxial strain, the maximum resulting stress (σ) can be estimated using the following linear eq 1[49]

$$\sigma(\text{MPa}) = -434\Delta\omega(\text{cm}^{-1}) \quad (1)$$

This gives a localized residual stress of ∼1.8 GPa, which corresponds to a strain (ε) of about 1.38% according to eq 2, and considering a Young's modulus $E_{[100]}$ of ∼130 GPa.[28,49]

$$\varepsilon(\%) = \sigma/\text{E} = -0.334\Delta\omega(\text{cm}^{-1}) \quad (2)$$

The most striking features characterized with μ-Raman spectroscopy are depicted in Figure 5c. The spectrum is composed of several broad bands with a massive peak between 400 and 550 cm^{-1}. This part of the spectra was deconvoluted into several components; the best fit obtained resulted in the sum of several Gaussian peaks and one Lorentzian peak at ∼522 cm^{-1} for c-Si (insert of Figure 5c.). Note in this case that the main c-Si peak is composed of two components resulting from deformation of the lattice (other deconvolutions did not fit). According to deconvolution and in agreement with the literature, this spectrum exhibits the features of amorphous Si (a-Si) in combination with a c-Si peak at ∼522 cm^{-1} generated from the surrounding crystalline Si. a-Si shifts are located at ∼481 cm^{-1} (TO mode), ∼380 cm^{-1} (longitudinal optic, LO mode), ∼310 cm^{-1} (longitudinal acoustic, LA mode), and one broad peak around ∼100−200 cm^{-1} (transverse acoustic, TA mode).[24,27−33,46] In general, the obtained μ-Raman spectra exhibited a background asymmetry and a width increase of the TO c-Si peak that further indicate the presence of an amorphous Si phase and strengthen the highlighted discrepancies of the Si bond lengths and angles.[27] Note that the a-Si observation is in agreement with the plastically deformed areas observed with SEM. The deconvolution spectra also show the presence of a peak at 514 cm^{-1}, which is typical for the presence of grain boundaries, or crystalline Si particles. A contribution of silica formation may also be involved during sonication processing; however, it is important to mention that its signature was not evidenced with μ-Raman, IR-TF, and X-ray reflectivity investigations. Note finally that the aging of the Si wafer in pure water during several days did not generate observable differences with the reference sample. The same remark rose when measuring after several hours in pure water on a nonactively sonicated area (e.g., side of the sample) or on a zone which was cut to fit the sample holder.

Amorphization of crystalline Si results from a structural destabilization of the Si structure and evidences a degree of atomic disorder at the surface of the sample.[32,33] This phenomenon can take place far below the melting temperature and has been reported to occur under several experimental conditions such as electron irradiation.[26] However, this phenomenon involves high energies (∼1 MeV) not reached in our study. Among the other reported methods, high-pressure investigations such as nanoindentation revealed an interesting way of amorphization through metallization of c-Si.[27−29,46] The high stress (∼9−16 GPa) provided to the crystal structure during indentation allows transformation of the cubic Si−I phase into a metastable metallic β-Sn phase (Si−II, body-centered tetragonal phase).[27−29] As a function of the pressure release, the metallic structure Si−II is able to lead to polymorphic metastable phases of crystalline Si−III (bc8, body-centered cubic structure, 8 atoms per unit cell) and Si-XII (r8, rhombohedral structure, 8 atoms per unit cell) phases but also to an amorphous Si phase (a-Si) or a mixture of both. The a-Si phase is favored during fast unloading processes, whereas the polymorphic phases are favored during slow release of pressure. Note that the deconvoluted spectra (Figure 5c) also showed a peak at ∼430 cm^{-1}, which can be attributed to bc8-type structure in accord with the literature.[27−29,32,33] The presence of the deformations (Supporting Information Figures SI.2 and SI.3) and the plastically deformed areas (Figure 2) observed with SEM, in combination with the spectroscopic observation of a-Si, and bc8 structure, suggest the possible Si amorphization through the metallic Si−II phase. It is important to emphasize that metallization of Si was reported to occur under Si compression with shock waves (evidenced with reflectivity and conductivity measurements).[50,51]

dx.doi.org/10.1021/jp305375r | J. Phys. Chem. C 2012, 116, 15493−15499

In a review devoted to the phase transformations of Si under contact, Domnich and Gogotsi concluded that Si phase transformation can be described as a deformation-induced transformation.[27−29] A thermodynamic nonequilibrium state of disorder equivalent to high-temperature amorphization may be generated during ultrasonic processing as it was, for example, reported for ball milling.[32,33] This amorphization may result from a loss of lattice stability during the cyclic compressions/decompressions of the collapsing bubbles.[27,29] It is important to emphasize that the range of pressure usually involved during these transformations is close to the pressures generated by the shock waves during sonication.[8] Acoustic cavitation is known to generate highly nonequilibrium conditions able to create transient decompression at the surface of the solid faster than what was observed by indentation. Combination of the lattice distortion with the generated compressive and shear strains induced by cavitation may therefore promote amorphization of the intervening material. Note that Si amorphization was recently reported to occur with electrosprayed nanodroplets bombarded toward a Si surface.[52]

TEM investigations confirmed the presence of a perfect diamond cubic single-crystalline structure for the nontreated sample devoid of phase transformation. Measurements carried out on the sonicated samples revealed the presence of a complex structure exhibiting complicated diffraction contrast because of the presence of a highly stressed and distorted structure (Figure 6, electron diffraction patterns inserted for each image). An increase of the apparent porosity of the resulting sample can also be underlined. The corresponding electron diffractograms suggested the presence of several phases: (i) the initial crystalline structure, (ii) wide diffuse rings resulting from a randomized distribution of Si atoms within the investigated structures and corresponding to the amorphous phase a-Si, and (iii) several concentric speckle-like halo rings typical for poly-Si. Therefore, TEM measurements were found to be consistent with the μ-Raman investigations. Correlation of the various experimental results indicates the presence of mixed domains composed of crystalline, amorphous, and polycrystalline phases. The presence of a transition stage where several phases are coexisting can be assumed. The presence of Si particles can result from fragmentation of c-Si with ultrasound and their embedding in an amorphous phase (a-Si or a-SiO_x) but also to partial recrystallization which may occur after amorphization and during sonication due to local sample heating and the generated solid frictions during erosion. A similar behavior was reported for the ball milling treatment of crystalline Si.[32,33]

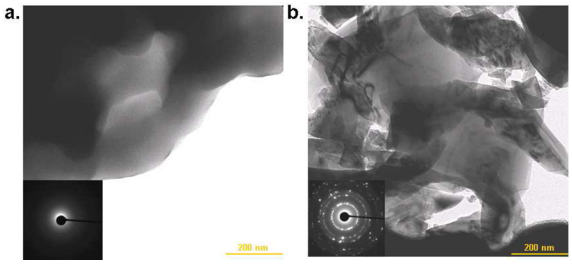

Figure 6. Bright-field TEM observation of a Si-sonicated area after 8 h of sonication (Ar, I_{ac} = 32 W cm^{-2}, 20 °C, H_2O, V = 250 mL) showing an amorphous Si structure (a) and a polycrystalline Si structure (b) with the corresponding electron diffraction patterns.

The different highlighted features evidence the complex stress state existing at the sonicated interface. According to the above observations, the mechanism of Ar excitation (Figure 1) results from the strains generated at the Si surface and in its crystalline structure. Indeed, Si phase transformation such as amorphization or metallization is known to go with a drastic change in density leading to volume expansion or contraction.[27−29,31] Therefore, these local transformations are able to fracture, deform, and dislocate the Si (sub)surface. In the mean time, the generated strains and distortions affect the electron density of states (thus affecting the thermal and electrical properties of silicon).[32,33] The introduced fractures induce a separation of the previously linked atoms responsible for a decrease of the wave function overlap across the crack. It results in creation of localized states associated with an increase of electron energy.[44] An electron hole recombination may then occur leading to the dielectric breakdown of the surrounding gas and de facto to the Ar* emission. Noteworthy, Ar* emission probably goes with Si emission usually observed around 1240 nm and between 3450 and 4965 nm.[26] Although Ar* transitions were observed, possible emission of the solid state component cannot be observed under these conditions since it occurs in a wavelength range not detected using our setup.

4. CONCLUSION

This work contributes to the understanding of the mechanism involved during cavitation at the solid−liquid interface following sonication at 20 kHz. High-power ultrasound was shown to induce interfacial changes of the physical, chemical, and structural properties of crystalline Si. Although cavitation erosion of Si involves formation of pits and cracks, its behavior under cavitation was found to be different from that observed on other materials such as glasses or metals. For the first time, ultrasound-induced mechanoluminescence is observed on an extended solid surface and a different mechanism of light emission is proposed. The gas discharge occurring at the solid−liquid interface opens new alternatives concerning monitoring of microscopic and macroscopic processes developed at the interface for medical, environmental, chemical, or engineering applications. Furthermore, spectroscopic and microscopic investigations strongly revealed the stress and dramatic transformations locally created during sonication. These properties may provide an interesting route of investigations devoted to the mechanical, electrical, and optoelectronic properties of Si (solar cells, transistors, MEMs, etc.).

■ ASSOCIATED CONTENT

Supporting Information

Additional spectra, AFM, and SEM pictures. This material is available free of charge via the Internet at http://pubs.acs.org.

■ AUTHOR INFORMATION

Corresponding Author

*E-mail: matthieu.virot@cea.fr.

Notes

The authors declare no competing financial interest.

■ ACKNOWLEDGMENTS

This study was carried out within the framework of the "Laboratoire Européen Associé SONO" which links the skills from ICSM Marcoule and MPI Potsdam-Golm. The authors

gratefully acknowledge Henri-Pierre Brau, Tony Chave, Sandrine Dourdain, Abdoul Aziz Ndiaye, and Renaud Podor for help in experiments and useful discussions.

REFERENCES

(1) Vinodgopal, K.; Neppolian, B.; Lightcap, I. V.; Grieser, F.; Ashokkumar, M.; Kamat, P. V. *J. Phys. Chem. Lett.* **2010**, *1*, 1987−1993.
(2) Bang, J. H.; Suslick, K. S. *Adv. Mater.* **2010**, *22*, 1039−1059.
(3) Patete, J. M.; Peng, X.; Koenigsmann, C.; Xu, Y.; Karn, B.; Wong, S. S. *Green Chem.* **2011**, *13*, 482−519.
(4) Gedanken, A. *Ultrason. Sonochem.* **2004**, *11*, 47−55.
(5) Suslick, K. S.; Flannigan, D. J. *Annu. Rev. Phys. Chem.* **2008**, *59*, 659−683.
(6) Leighton, T. G. *The Acoustic Bubble*; Academic Press: London, 1994.
(7) Suslick, K. S. Sonoluminescence and Sonochemistry. In *Encyclopedia of Physical Science and Technology*, 3rd ed.; Meyers, R. A., Ed.; Academic Press: San Diego, CA, 2001.
(8) Virot, M.; Chave, T.; Nikitenko, S. I.; Shchukin, D. G.; Zemb, T.; Mohwald, H. *J. Phys. Chem. C* **2010**, *114*, 13083−13091.
(9) Török, B.; Balázsik, K.; Felföldi, K.; Bartók, M. *Ultrason. Sonochem.* **2001**, *8*, 191−200.
(10) Skorb, E. V.; Andreeva, D. V.; Möhwald, H. *Angew. Chem., Int. Ed.* **2012**, *51*, 5138−5142.
(11) Rivas, D. F.; Prosperetti, A.; Zijlstra, A. G.; Lohse, D.; Gardeniers, H. J. G. E. *Angew. Chem., Int. Ed.* **2010**, *49*, 9699−9701.
(12) Belova, V.; Gorin, D. A.; Shchukin, D. G.; Möhwald, H. *Angew. Chem., Int. Ed.* **2010**, *49*, 7129−7133.
(13) Virot, M.; Pflieger, R.; Ravaux, J.; Nikitenko, S. *J. Phys. Chem. C* **2011**, *115*, 10752−10756.
(14) Eddingsaas, N. C.; Suslick, K. S. *Nature* **2006**, *444*, 163.
(15) Eddingsaas, N. C.; Suslick, K. S. *J. Am. Chem. Soc.* **2007**, *129*, 6718−6719.
(16) Eddingsaas, N. C.; Suslick, K. S. *Phys. Rev. Lett.* **2007**, *99*, 234301.1−4.
(17) Sharipov, G. L.; Abdrakhmanov, A. M.; Tukhbatullin, A. A. *Tech. Phys. Lett.* **2009**, *35*, 452−455.
(18) Sharipov, G. L.; Tukhbatullin, A. A.; Abdrakhmanov, A. M. *Prot. Met Phys. Chem. Surf.* **2011**, *47*, 13−19.
(19) Schmidt, V.; Wittemann, J. V.; Gösele, U. *Chem. Rev.* **2010**, *110*, 361−388.
(20) Spinelli, P.; Verschuuren, M. A.; Polman, A. *Nature* **2012**, *3*, 692.
(21) Kumar, P.; Kiran, M. S. R. N. *Sci. Technol. Adv. Mater.* **2010**, *11*, 025003.1−8.
(22) Derkacs, D.; Lim, S. H.; Matheu, P.; Mar, W.; Yu, E. T. *Appl. Phys. Lett.* **2006**, *89*, 093103.1−3.
(23) Monroy, B. M.; Remolina, A.; García-Sánchez, M. F.; Ponce, A.; Picquart, M.; Santana, G. *J. Nanomater.* **2011**, 190632.1−9.
(24) Gajović, A.; Gracin, D.; Juraić, K.; Sancho-Parramon, J.; Čeh, M. *Thin Solid Films* **2009**, *517*, 5453−5458.
(25) Viera, G.; Mikikian, M.; Bertran, E.; Roca i Cabarrocas, P.; Boufendi, L. *J. Appl. Phys.* **2002**, *92*, 4684−4694.
(26) Yamasaki, J.; Takeda, S.; Tsuda, K. *Phys. Rev. B.* **2002**, *65*, 115213.1−10.
(27) Domnich, V.; Gogotsi, Y. *Rev. Adv. Mater. Sci.* **2002**, *3*, 1−36.
(28) Das, C. R.; Hsu, H. C.; Dhara, S.; Bhaduri, A. K.; Raj, B.; Chen, L. C.; Chen, K. H.; Albert, S. K.; Ray, A.; Tzeng, Y. *J. Raman Spectrosc.* **2010**, *41*, 334−339.
(29) Wermelinger, T.; Spolenak, R. *J. Raman Spectrosc.* **2009**, *40*, 679−686.
(30) Stopford, J.; Allen, D.; Adrian, O.; Morshed, M.; Wittge, J.; Danilewsky, A. N.; McNally, P. J. *Microelectron. Eng.* **2011**, *88*, 64−71.
(31) Tanikella, B. V.; Somasekhar, A. H.; Sowers, A. T.; Nemanich, R. J.; Scattergood, R. O. *Appl. Phys. Lett.* **1996**, *69*, 2870−2872.
(32) Unifantowicz, P.; Vaucher, S.; Lewandowska, M.; Kurzydłowski, K. J. *J. Phys.: Condens. Matter* **2008**, *20*, 025205.1−5.
(33) Morris, M. A.; Morris, D. G. *J. Mater. Sci.* **1991**, *26*, 4687−4696.
(34) Deymier, P. A.; Khelif, A.; Djafari-Rouhani, B.; Vasseur, J. O.; Raghavan, S. *J. Appl. Phys.* **2000**, *88*, 2423−2429.
(35) Podolian, A.; Nadtochiy, A.; Kuryliuk, V.; Korotchenkov, O.; Schmid, J.; Drapalik, M.; Schlosser, V. *Sol. Energy Mater. Sol. Cells* **2011**, *95*, 765−772.
(36) El-Bahar, A.; Stolyarova, S.; Chack, A.; Weil, R.; Beserman, R.; Nemirovsky, Y. *Phys. Status Solidi* **2003**, *197*, 340−344.
(37) Kalem, S.; Yavuzcetin, O.; Altineller, C. *J. Porous Mater.* **2000**, *7*, 381−383.
(38) Kayahan, E. *Appl. Surf. Sci.* **2011**, *257*, 4311−4316.
(39) Koshka, J.; Ostapenko, S.; Ruf, T.; Zhang, J. M. *Appl. Phys. Lett.* **1996**, *69*, 2537−2539.
(40) Pflieger, R.; Brau, H.-P.; Nikitenko, S. I. *Chem.—Eur. J.* **2010**, *16*, 11801−11803.
(41) Nikitenko, S. I.; Venault, L.; Moisy, P. *Ultrason. Sonochem.* **2004**, *11*, 139−142.
(42) Suslick, K. S.; Flannigan, D. J. *Annu. Rev. Phys. Chem.* **2008**, *59*, 659−683.
(43) Bruggeman, P. D.; Schram, D. C.; Kong, M. G.; Leys, C. *Plasma Process. Polym.* **2009**, *6*, 751−762.
(44) Chandra, B. P.; Patel, R. P.; Gour, A. S.; Chandra, V. K.; Gupta, R. K. *J. Lumin.* **2003**, *104*, 35−45.
(45) Skorb, E. V.; Shchukin, D. G.; Möhwald, H.; Andreeva, D. V. *Nanoscale* **2010**, *2*, 722−727.
(46) Li, X.; Lu, J.; Yang, S. *Tribol. Int.* **2009**, *42*, 628−633.
(47) Anastassakis, E. *J. Appl. Plys* **1999**, *86*, 249−257.
(48) De Wolf, I. *Semicond. Sci. Technol.* **1996**, *11*, 139−154.
(49) Himcinschi, C.; Reiche, M.; Scholz, R.; Christiansen, S. H.; Gösele, U. *Appl. Phys. Lett.* **2007**, *90*, 231909.1−3.
(50) Zaporozhets, Y. B.; Mintsev, V. B.; Fortov, V. E. *Sov. Tech. Phys. Lett.* **1987**, *13*, 83−84.
(51) Gilev, S. D.; Trubachev, A. M. *J. Phys.: Condens. Matter* **2004**, *16*, 8139−8153.
(52) Gamero-Castaño, M.; Torrents, A.; Valdevit, L.; Zheng, J.-G. *Phys. Rev. Lett.* **2010**, *105*, 145701.1−4.